Powder X-Ray Diffraction, Applications

Daniel Louër, Université de Rennes, CNRS, France

© 1999 Elsevier Ltd. All rights reserved.

This article is reproduced from the previous edition, volume 3, pp 1865–1875, © 1999, Elsevier Ltd.

Symbols

A_n, B_n	Fourier coefficients
A^D	distortion coefficient
A^S	size coefficient
B	isotropic atomic displacement
d	interlayer spacing
D	crystallite diameter
e	microstrain
f	atomic scattering factor
F	structure factor
h,k,l	Miller indices
I	intensity
Lp	angle-dependent factor
m	Pearson exponent
M_{20}	de Wolff figure of merit
m_k	reflection multiplicity
N	site occupation factor
R	goniometer circle radius
R_p	profile factor
s	scale factor
W	weight fraction
Z	number of molecules per unit cell
β	integral breadth
δ	specimen displacement
ε	apparent crystallite size
η	pseudo-Voigt mixing factor
θ	diffraction angle
λ	wavelength
ϕ	shape factor
Φ	line-profile function

Introduction

X-ray powder diffraction is a nondestructive technique widely used for the characterization of micro-crystalline materials. The method has been traditionally applied for phase identification, quantitative analysis and the determination of structure imperfections. More recently, applications have been extended to new areas, such as the determination of moderately complex crystal structures and the extraction of three-dimensional microstructural properties. This is the consequence of the higher resolution of modern diffractometers, the advent of high-intensity X-ray sources and the development of line-profile modelling approaches to overcome the line overlap problem arising from the one-dimensional data contained in a powder diffraction pattern. The method is normally applied to data collected at room temperature. Nevertheless, it is also used with data collected *in situ* as a function of an external constraint (temperature, pressure, electric field, atmosphere, etc.), offering a useful tool for the interpretation of chemical reaction mechanisms and materials behaviour. Various kinds of microcrystalline materials may be characterized from X-ray powder diffraction, such as inorganic, organic and pharmaceutical compounds, minerals, catalysts, metals and ceramics. For most applications, the amount of information which can be extracted depends on the nature and magnitude of the microstructural properties of the sample (crystallinity, structure imperfections, crystallite size), the complexity of the crystal structure and the quality of the experimental data (instrument performance, counting statistics).

Line Profile Parameters

The observed diffraction line profiles are distributions of intensities $I(2\theta)$ defined by several parameters. The most commonly used measure for the reflection angle is the *position* $2\theta_0$ of the maximum intensity (I_0). It is related to the lattice spacing d of the diffracting hkl plane and the wavelength λ by Bragg's law.

$$\lambda = 2d \sin\theta$$

The *dispersion* of the distribution, or diffraction line broadening, is measured by the full width at half the maximum intensity (FWHM) or by the integral breadth (β) defined as the integrated intensity (I) of the diffraction profile divided by the peak height ($\beta = I/I_0$). Line broadening arises from the convolution of the spectral distribution with the functions of instrumental aberrations and sample-dependent effects (crystallite size and structure imperfections). Since Fourier-series methods play an important role in X-ray diffraction by imperfect solids, the coefficients (A_n, B_n) of the Fourier series used to represent a line profile are also characteristics of the line broadening. The line *shape factor* is described by the ratio ϕ of the FWHM to the integral breadth ($\phi = \mathrm{FWHM}/\beta$). There are alternative shape factors according to the analytical functions Φ, given in

Table 1 Some flexible line-profile functions $\Phi(x)$ used to model powder diffraction line profiles (L and G denote the Lorentzian and Gaussian functions, respectively)

Name	*Function*	*Shape factor*
Pseudo-Voigt (p-V)	$C_1[\eta L+(1-\eta)G]$ (η,C_1: adjustable parameters)	*Mixing factor* η η=1 Lorentzian shape η=0: Gaussian shape $\eta>1$: super-Lorentzian shape
Pearson VII (PVII)	$C_2(1+Cx^2)^{-m}$ (m, C, C_2: adjustable parameters)	*Exponent m* m=1: Lorentzian shape $m=\infty$: Gaussian shape $m<1$: super-Lorentzian shape
Voigt (V)	$C_3\int L(x')G(x-x')dx'$ (C_3: adjustable parameter)	ϕ=FWHM/β ϕ=0.636 6: Lorentzian shape ϕ=0.939 4: Gaussian shape

Table 1, commonly used for modelling individual diffraction lines, e.g. the mixing factor η for the pseudo-Voigt and the exponent m for the Pearson VII. The *area* is defined by the integrated intensity I of the diffraction line. It is related to the atomic content and arrangement in the unit cell, to the amount of diffracting sample and to angle-dependent factors (Lp). It is proportional to the square of the structure factor amplitude F_{hkl}:

$$F_{hkl}=\Sigma_j N_j f_j \exp 2\pi i(hx_j+ky_j+lz_j) \times \exp(-B_j \sin^2\theta/\lambda^2)$$

where N_j is the site occupation factor, f_j is the atomic scattering factor, B_j is the isotropic atomic displacement (thermal) parameter, h, k and l are the Miller indices, and x_j, y_j and z_j are the position coordinates of atom j in the unit cell. Table 2 lists the specific applications of the powder diffraction method according to the line-profile parameters.

Table 2 Main applications of X-ray powder diffraction

Diffraction line parameter	*Applications*
Peak position	Unit-cell parameter refinement Pattern indexing Anisotropic thermal expansion Homogeneous stress Phase identification
Line intensity	Phase abundance Chemical reaction kinetics Crystal-structure determination and refinement (whole pattern) Search/match ($d-I$) Space-group determination ($2\theta_0$-absent I_{hkl}) Preferred orientation
Line width and shape	Instrumental resolution function Microstructure
Line-profile broadening	Microstructure (crystallite size, size distribution, lattice distortion, structure mistakes, dislocations, composition gradient), crystallite growth kinetics

Diffraction Geometry and Data Collection

For most applications it is essential that the powder diffraction data be collected appropriately. Therefore, it is of prime importance to spend time optimizing the adjustment of the diffractometer, the quality of the radiation employed and the randomization of the crystallites in the sample. There are several designs for X-ray powder diffractometers (reflection or transmission modes), each of them having advantages and disadvantages. Figure 1 shows an optics arrangements commonly used with conventional divergent-beam X-ray sources, based on the Bragg–Brentano parafocusing geometry. The beam converges on the receiving slit after diffraction by the sample. The geometry is characterized by two circles, the goniometer circle with a constant radius R and the focusing circle with a radius dependent on θ. It uses a flat sample which lies tangentially to the focusing circle. The main advantage of this reflection geometry is that no absorption correction has to be made if an 'infinitely' thick sample is used. Disadvantages are that by using a flat sample, preferred orientation effects are increased and at low angles the illuminated area can become larger than the sample. Preferred orientation effects can be reduced by using side-loaded sample holders. The most frequent angular errors arise from a shift of the zero-2θ position and a displacement δ of the specimen from the goniometer axis of rotation ($\Delta 2\theta=2\delta\cos\theta/R$). Transmission geometry, often combined with a position-sensitive detector (PSD), can be employed with thin flat samples or capillaries. The main advantages are the small amount of sample used and, with capillaries, the reduction of preferred orientation. Transmission optics

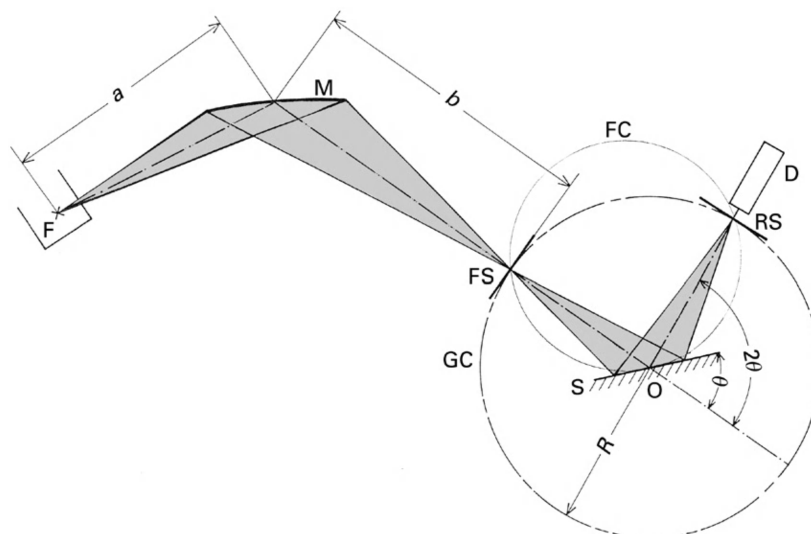

Figure 1 Optics of a conventional focusing powder diffractometer with monochromatic X-rays (Bragg–Brentano geometry with a reflection specimen): F line focus of X-ray tube, M incident-beam monochromator, *a* short focal distance, *b* long focal distance, FS focal slit, S flat specimen, GC goniometer circle, O goniometer axis, R goniometer radius, FC focusing circle, θ Bragg angle, 2θ reflection angle, RS receiving slit, D detector.

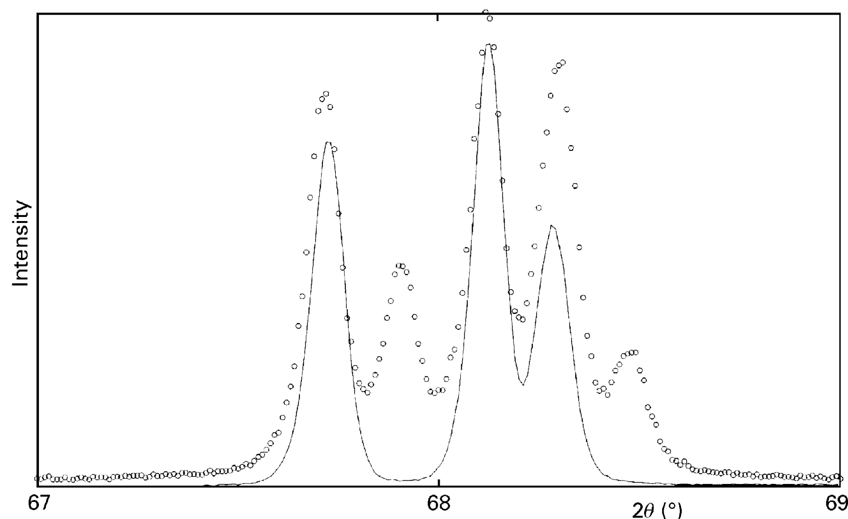

Figure 2 The quartz cluster of reflections 212, 203 and 301 collected with Cu$K\alpha_1$ radiation (continuous line) and with the Cu$K\alpha_1$–$K\alpha_2$ doublet (circles).

are ideal for 'transparent' materials, containing only light atoms, but for highly absorbing materials, patterns are difficult to measure. X-ray synchrotron radiation presents some important advantages over conventional X-ray sources. The excellent angular collimation combined with the wavelength tunability and high brightness of the synchrotron source make it ideal for many types of X-ray diffraction experiments. Moreover, with parallel-beam optics, sample-displacement aberrations in diffraction lines are completely eliminated.

Although a basic requirement of the Bragg law is the use of monochromatic radiation, the doublet $K\alpha_1$–$K\alpha_2$ from copper is the most popular wavelength used with laboratory diffractometers. However, for the more demanding applications it is desirable to remove the $K\alpha_2$ component with a monochromator located in the incident beam (Figure 1). There is some reduction in the intensity of $K\alpha_1$, but the number of reflections in the pattern is halved and thereby the degree of line overlap is reduced. Figure 2 shows the improvement in resolution achieved with the monochromatic Cu$K\alpha_1$ radiation ($\lambda = 1.5406$ Å) with respect to the $K\alpha_1$–$K\alpha_2$ doublet.

The performances of powder diffractometers are determined by the precision of peak position

measurements and the instrument resolution function (IRF), normally expressed by the angular dependence of the FWHM obtained with a reference material. The most widely used standard reference materials (SRMs) for diffractometer characterization are those from the National Institute of Standards and Technology (NIST). For instance, powders of Si (SRM 640 b, $a = 5.430940 \pm 0.000035$ Å) and fluorophlogopite mica (SRM 675, interlayer spacing $d_{001} = 9.98104 \pm 0.00007$ Å) are proposed as *d*-spacing standards, while LaB_6 (SRM 660) is recommended as a line-profile standard. With laboratory X-ray diffractometers errors on peak positions can be less than $0.01°(2\theta)$ and the IRF has typically a minimum around $0.06°(2\theta)$ at intermediate angles, increasing to twice this value at $\sim 130°(2\theta)$ as a consequence of spectral dispersion. The best instrumental resolution (~ 0.01–$0.02° 2\theta$) is obtained with the synchrotron parallel beam optics with a crystal analyser mounted in the diffracted beam. This is of particular interest in some applications, such as the study of complex crystal structures.

Pattern Modelling

Pattern modelling techniques are used in most current applications. The intensity at point x_i in the calculated pattern is given by

$$y_{\mathrm{cal}}(x_i) = \sum_k I_k \Phi(x_i - x_k) + b(x_i)$$

where I_k is the integrated intensity of reflection k, Φ is one of the normalized profile functions given in Table 1 and $b(x_i)$ is the background contribution. The summation is over all reflections contributing to the intensity at point x_i. Parameters defining the model are refined until the quantity

$$S = \sum w(x_i)[y_{\mathrm{obs}}(x_i) - y_{\mathrm{cal}}(x_i)]^2$$

is a minimum, the summation being over all data points in the diffraction pattern with $w(x_i)$ being the appropriate weighting factor. Although a visual inspection of the difference curve between observed and calculated patterns is the best way to judge the quality of the fit over the whole angular range, numerical factors are used to assess the quality of the final refinement. These are listed in Table 3.

Pattern Decomposition

This is a systematic procedure for decomposing a powder pattern into its component Bragg reflections without reference to a structure model and, thereby, line-profile parameters ($2\theta_0$, I_0, I, FWHM, β, shape factors) are extracted. Figure 3 shows the fitting of pseudo-Voigt functions to the individual lines of the pattern of a ZnO sample displaying diffraction line broadening. However, for extracting integrated intensities over the complete pattern, for a subsequent structural analysis, an approach incorporating constrained peak positions, according to the refined unit-cell dimensions and to the space group, allows the generation of only space-group allowed intensities.

Table 3 Some numerical criteria of fit used in pattern-fitting methods

R-profile	$R_p = \dfrac{\sum \lvert y_i(\mathrm{obs}) - y_i(\mathrm{cal}) \rvert}{\sum y_i(\mathrm{obs})}$
R-weighted profile	$R_{wp} = \left[\dfrac{\sum \lvert w_i [y_i(\mathrm{obs}) - y_i(\mathrm{cal})] \rvert^2}{\sum w_i [y_i(\mathrm{obs})]^2}\right]^{1/2}$
R-structure factor	$R_F = \dfrac{\sum \left\lvert I_{hkl}(\text{‘obs’})^{1/2} - I_{hkl}(\mathrm{cal})^{1/2} \right\rvert}{\sum I_{hkl}(\text{‘obs’})^{1/2}}$
R-Bragg factor	$R_B = \dfrac{\sum \lvert I_{hkl}(\text{‘obs’}) - I_{hkl}(\mathrm{cal}) \rvert}{\sum I_{hkl}(\text{‘obs’})}$

The Rietveld Method

In the Rietveld method an observed and a calculated powder diffraction pattern are compared and the difference is used to refine the atomic coordinates of the structure model. The calculated intensity at point x_i is given by the equation

$$y_{\mathrm{cal}}(x_i) = s \sum_k m_k (Lp)_k |F_k|^2 P_k \Phi(x_i - x_k) + b(x_i)$$

where s is a scale factor, m_k is the reflection multiplicity and P_k is a function to deal with the preferred orientation of the crystallites. They are two groups of refined parameters arising from the structure model (atomic coordinates x_j, y_j and z_j, atomic displacement parameters, unit-cell dimensions) and the instrumental model (angular dependence of the profile parameters, FWHM and shape factors, 2θ-zero position, preferred orientation, etc.). Recommendations for Rietveld-refinement strategies have been formulated by the Commission on Powder Diffraction of the International Union of Crystallography. Figure 4 shows a typical final Rietveld plot obtained from powder data collected with the capillary method. The precision of a structure refinement depends on many factors, e.g. the number of parameters to be refined, data quality (preferred orientation, counting statistics, anisotropic line broadening), the contrast between atoms and the size of the unit cell. Moreover, structure refinement from X-ray diffraction data is strongly influenced by the fall-off of the scattering atomic

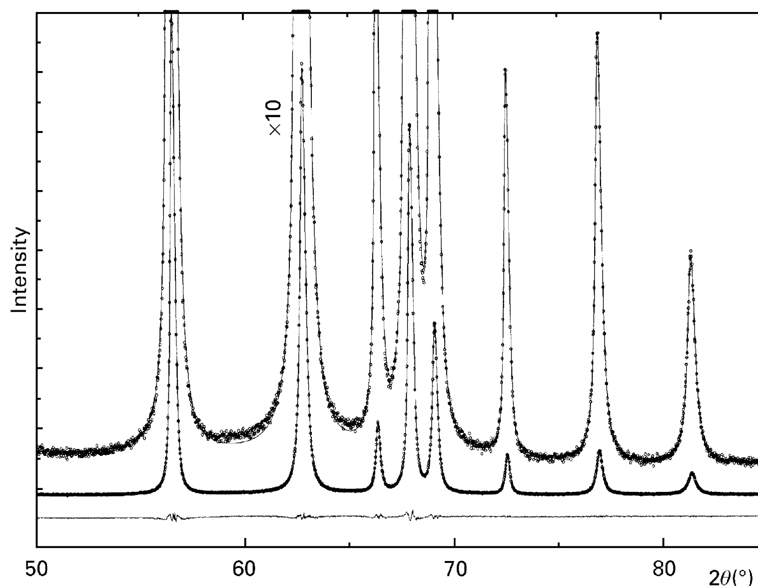

Figure 3 Fitting of a part of the pattern of a sample of nanocrystalline ZnO, using pseudo-Voigt functions for modelling individual diffraction lines, Cu$K\alpha_1$ radiation, R_{wp}=1.2%. The observed intensity data are plotted as circles and the calculated pattern is shown as a continuous line. The lower trace is the difference curve. The ×10 scale expansion shows the fit in the line-profile tails.

factors f_j with d^{-1} (or 2θ). This is in contrast with neutron-diffraction data, for which the scattering length does not fall off significantly over the range of observations. Another important difference between neutron and X-ray diffraction is that the relative scattering powers of atoms for neutrons and X-rays are significantly different. With neutrons there are pronounced differences in the scattering lengths of neighbouring elements. In the case of X-rays, there is a monotonic variation in X-ray scattering factors and hence light atoms are weak X-ray scatterers. For instance, in the case of $U(UO_2)(PO_4)_2$ the X-ray powder data are dominated by the U atom, the ratio of the scattering factors of U to O being greater than 11.5, while with neutrons oxygen is a relatively strong scatterer and then the ratio of the appropriate scattering lengths is 1.45. This property explains the major role played by neutron powder diffraction in determining oxygen content and position in high T_c cuprates in the presence of heavy atoms such as Ba, Hg, Tl and Bi.

Qualitative and Quantitative Analyses

Phase Identification

Qualitative phase identification is traditionally based on a comparison of observed data with interplanar spacings d and relative intensities I_0 compiled for crystalline materials. The Powder Diffraction File (PDF), edited by the International Centre for Diffraction Data (ICDD, www.icdd.com), contains powder data for more than 600 000 substances. It includes nearly as many inorganic as organic molecules. The Boolean search program supplied by the ICDD with the database offers great flexibility in phase identification and characterization. In a more recent search/match procedure, complete digitized observed diffraction patterns are used, instead of simply a list of extracted *d*s and *I*s. To decide whether or not the pattern contains the data of a particular PDF entry, its data are compared with parts of zero intensity in the pattern for the unknown substance. The method can be used for multiphase patterns. As each phase is identified, the diffraction lines can be removed and the procedure is repeated by using the remaining regions of the pattern. The method is very efficient, even for the identification of minor phases if some known chemical constraints are introduced into the search.

Quantitative Phase Abundance

Quantitative phase analysis is the determination of the amounts of different phases present in a sample. The powder diffraction method is widely used to determine the abundance of distinct crystalline phases, e.g. in rocks and in mixtures of polymorphs, such as zirconia ceramics. The principle of the method is straightforward; the integrated intensity (I) of the diffraction lines from any phase in a mixture is proportional to the mass of the phase present in the sample. One analytical approach is based on a reference-intensity ratio (RIR) defined as the integrated intensity of the strongest reflection for the phase of interest to the strongest line of a standard (usually the 113 reflection of corundum) for a 1:1 mixture by weight. The measurement and use of RIRs is straightforward for materials for which the intensity does

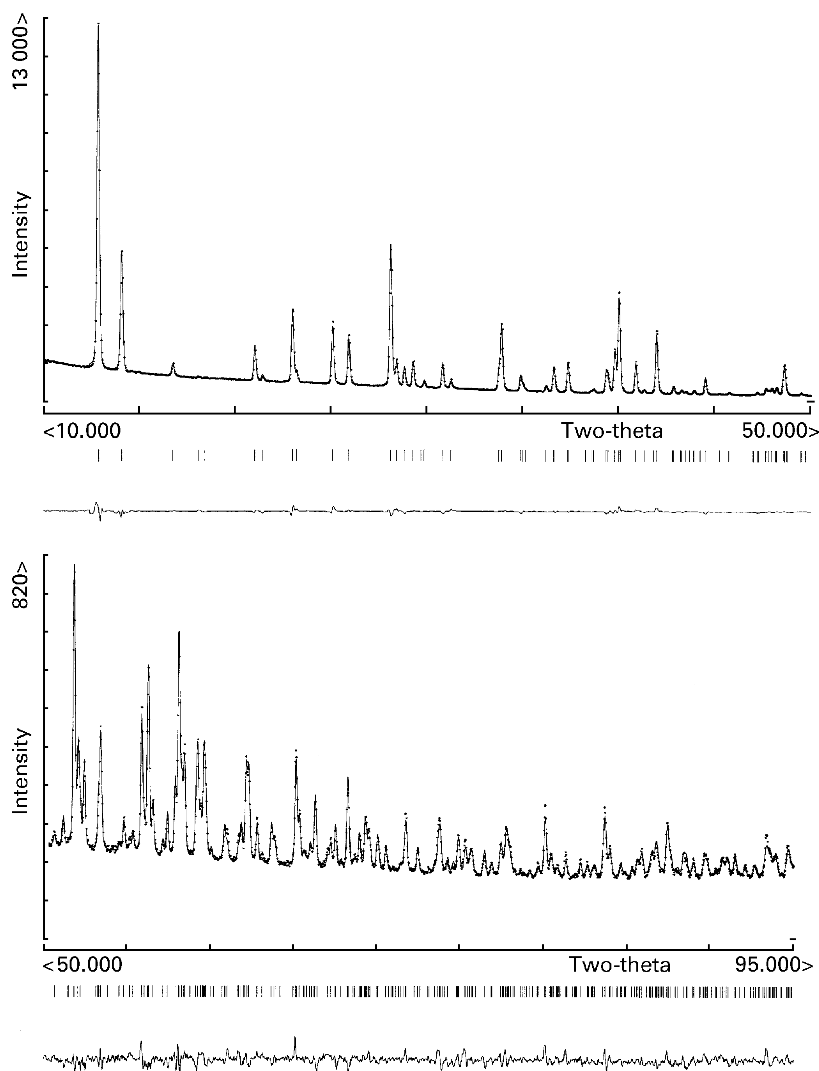

Figure 4 Example of a typical Rietveld plot. The powder data of $LiB_2O_3(OH) \cdot H_2O$ were collected with the Debye–Scherrer (capillary) geometry using monochromatic Cu$K\alpha_1$ radiation and a curved position-sensitive detector. The observed data are plotted as points and the calculated pattern as a continuous line. The lower trace is a plot of the difference of observed minus calculated. The vertical markers indicate the positions of calculated Bragg reflections. The intensity scale is magnified for the high-angle part, where the intensity of observed diffraction lines is low. Reprinted with permission of the International Union of Crystallography from Louër D, Louër M, and Touboul M (1992) Crystal structure determination of lithium diborate hydrate, $LiB_2O_3(OH) \cdot H_2O$, from X-ray powder diffraction data collected with a curved position-sensitive detector. *Journal of Applied Crystallography* 25: 617–623.

not vary with composition and preferred orientation. Because of the potential health hazard of respirable crystalline silica, X-ray powder diffraction is also used for detecting, identifying and quantifying the crystalline and amorphous silica of all types of samples from airborne dusts to bulk commercial products. SRMs 1878 (α-quartz) and 1979 (cristobalite) from NIST are certified with respect to amorphous content for analysis of silica-containing materials in accordance with health and safety regulations.

An extension of the Rietveld method is its application to multiphase samples for the determination of phase abundance. There is a simple relationship between the individual scale factors determined in a Rietveld analysis and the weight fractions (W_i) of the phase concentration in a multicomponent mixture:

$$W_i = s_i(ZMV)_i / \sum_j s_j(ZMV)_j$$

where s_i, Z_i, M_i and V_i are the scale factor, the number of molecules per unit cell, the mass of the formula unit and

the unit-cell volume of phase i, respectively and the summation is over all phases present. A requirement of the method is that the crystal structure is known for each phase in the mixture. The use of all reflections in the selected angular range is a great advantage, since the uncertainty on phase abundance is reduced by minimizing preferred orientation effects. In general, phase-analysis results obtained with X-ray data are inferior to those obtained from neutron data. This is related to residual errors arising from an imperfect preferred orientation modelling and from microabsorption effects.

Ab Initio Structure Determination

Among the most recent advances of the powder method is the determination of crystal structures from powder diffraction data. It is an application for which the resolution of the pattern is of prime importance. A series of successive stages are involved in the analysis, including the determination of cell dimensions and identification of the space group from systematic reflection absences, the extraction of structure factor moduli $|F_{hkl}|$, the solution to the phase problem to elaborate a structure model and, finally, the refinement of the atomic coordinates with the Rietveld method.

Pattern Indexing

The purpose of pattern indexing is to reconstruct the three-dimensional reciprocal lattice of a crystalline solid from the radial distribution of lengths $d^*(=1/d)$ of the diffraction vectors. The basic equation used for indexing a powder diffraction pattern is obtained by squaring the reciprocal-lattice vectors $\mathbf{d}_{hkl}{}^*(=h\mathbf{a}^* + k\mathbf{b}^* + l\mathbf{c}^*)$, expressed in terms of the basis vectors of the reciprocal lattice ($\mathbf{a}^*$, $\mathbf{b}^*$, $\mathbf{c}^*$) and hkl Miller indices,

$$Q(hkl) = h^2Q_A + k^2Q_B + l^2Q_C + 2klQ_D + 2hlQ_E + 2hkQ_F$$

where $Q(hkl)=1/d^2$, $Q_A=a^{*2}$, $Q_B=b^{*2}$, $Q_C=c^{*2}$, $Q_D=b^*c^*\cos\alpha^*$, $Q_E=c^*a^*\cos\beta^*$, $Q_F=a^*b^*\cos\gamma^*$; a^*, b^*, c^* are the linear parameters and α^*, β^*, γ^* the angles of the reciprocal unit cell. This quadratic form corresponds to the triclinic crystal symmetry. Only four parameters are required for a monoclinic cell, three for an orthorhombic cell, two for tetragonal and hexagonal cells, and one for a cubic cell. Indexing a powder pattern consists in finding the linear and angular dimensions of the unit cell, from which a set of Miller indices hkl can be assigned to each observed line Q_{obs}, within the experimental error on the observed peak positions. Automatic procedures are available to index a powder diffraction pattern. They are based on three main approaches, regardless of symmetry: the zone-indexing method, the index-permutation method and the successive-dichotomy method. The use of pattern-indexing methods requires a high precision on peak positions ($|\Delta 2\theta| < 0.03°2\theta$). The assessment of the reliability of an indexed pattern is carried out with the de Wolff figure of merit M_{20}:

$$M_{20} = Q_{20}/2\langle\Delta Q\rangle N_{cal}$$

where Q_{20} corresponds to the 20th observed line, $\langle\Delta Q\rangle$ is the average absolute discrepancy between $Q_{k\text{obs}}$ and the nearest $Q_{k\text{cal}}$ value and N_{cal} is the number of distinct calculated Q values smaller than Q_{20}, not including any systematic absences if they are known. M_{20} is greater when $\langle\Delta Q\rangle$ is small and N_{cal} is as close as possible to 20. A related figure of merit, F_N, introduced for the evaluation of powder data quality, is also used. It is reported as 'value ($\langle\Delta 2\theta\rangle$, N_{cal})', where $\langle\Delta 2\theta\rangle$ is the average angular discrepancy. A solution with M_{20} greater than 20 is generally correct, although some geometrical ambiguities or the presence of a dominant zone can mask the true solution. An additional check of the reliability of the solution consists in indexing all measurable peak positions in the pattern, from which systematic absent reflections can be detected and, then, possible space groups are proposed. With synchrotron parallel-beam optics, higher figures of merit are obtained, since angular precision and resolution (more lines are observed) are considerably improved. There is no particular problem for indexing, from conventional X-ray data, patterns of materials with moderate cell volumes and, for instance, patterns of monoclinic compounds with volumes up to 3000 Å^3 can be normally handled.

Structure Solution

Following the determination of the unit cell and space group assignment, integrated intensities (I_{hkl}) (or structure factor amplitudes) are extracted with a pattern-decomposition technique. For clusters of overlapping lines an equipartition of the overall intensity is generally applied. Therefore, intensity data sets contain a limited number of unambiguously measured reflections. An estimation of the proportion of statistically independent reflections can be calculated from an algorithm based on line width and reflection proximity. It is a useful indicator which depends on the selected angular range. The methods for solving the phase problem used with single-crystal data (Patterson methods and direct methods) are generally applicable with powder data. Computer programs have been adapted to the powder diffraction case. In general, only fragments of the structure are found from these methods; the remaining atoms are then obtained from subsequent Fourier calculations. However, with good data and a favourable proportion of

unambiguous reflections, the success of the direct methods can be very high and even complete models (non-H atoms) may be revealed from one calculation. Considerable effort has been devoted to the development of new approaches for the treatment of powder-diffraction data. They include the Monte Carlo and the simulated annealing approaches, the maximum-entropy method, the atom-atom potential method and genetic algorithms. Computer-modelling approaches operate in direct space. Trial crystal structures are generated independently of the observed powder diffraction data. The suitability of each structure model is assessed by comparison between the calculated and observed diffraction patterns and is quantified using an appropriate profile
R-factor (see **Table 3**). The direct-space methods present the advantage of avoiding the critical stage of extracting the individual intensities from pattern decomposition. They are suitable for organic molecules, but a detailed knowledge of the expected molecule (bond lengths and torsional angles) is a basic requirement. An example is the structure determination of a metastable form of piracetam, $C_6H_{10}N_2O_2$, whose lifetime at room temperature is only 2 h, solved from powder data collected with a PSD (**Figure 5**). Structure determination from powder data is used in varied fields of materials science, including inorganic, organometallic and organic chemistry, mineralogy and pharmaceutical science. Although the analysis is generally applicable to moderately complex structures, it has been successful for solving structures containing, for instance, 29 atoms in the asymmetric unit, e.g. $Ga_2(HPO_3)_3 \cdot 4H_2O$, Ba_3AlF_3, $Bi(H_2O)_4(OSO_2CF_3)$, or having a high unit-cell volume, e.g. 7471 Å^3 for $[(CH_3)_4N]_4Ge_4S_{10}$. With the ultra-high resolution available with X-ray synchrotron radiation, determination of more complex structure can now be undertaken, particularly with materials containing light atoms.

For specific applications, the tunability of synchrotron radiation sources allows the X-ray wavelength to be changed readily, and this can be exploited to enhance the contrast between close elements in the periodic table. These studies are termed anomalous (resonant) scattering experiments. The atomic scattering factor for X-rays is defined as

$$f = f_0(\theta) + f'(E) + \mathrm{i}f''(E)$$

where f_0 varies only with $\sin\theta/\lambda$ and f' and f'' are the energy-dependent real and imaginary parts of the anomalous contribution. By selecting a wavelength close to the absorption edge of an element the scattering factor may change by a few electrons. By comparing powder data collected near-edge and off-edge, the technique can be used to determine the distribution of cations with similar atomic numbers over crystallographically distinct sites. Applications can be extended to mixed-oxidation states of an absorbing element if these are ordered within a crystal structure, e.g. Eu^{2+} and Eu^{3+} in Eu_3O_4 or Ga^+ and Ga^{3+} in $GaCl_2$.

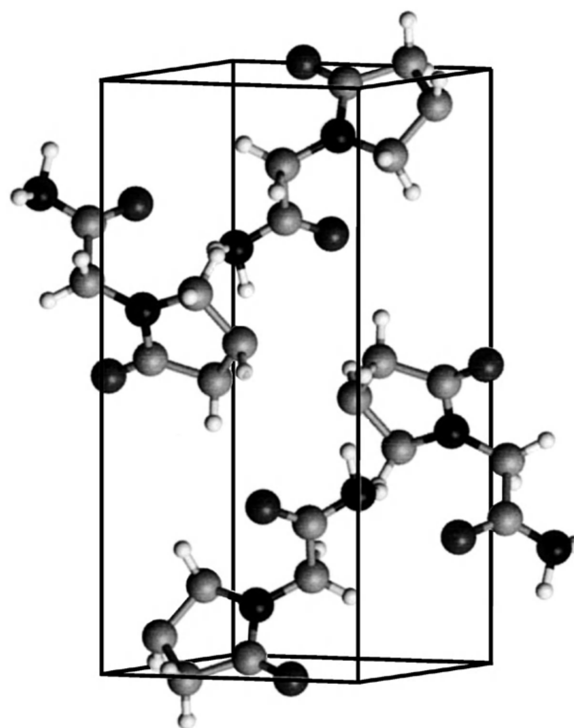

Figure 5 View of the crystal structure of a metastable phase of piracetam, $C_6H_{10}N_2O_2$, solved from the atom–atom potential method and refined with the Rietveld method. The crystal symmetry is monoclinic, space group $P2_1/n$ (the unit cell is shown with the *a* axis horizontal and *b* axis vertical) (crystal data are reported in *Acta Crystallographica* B51: 182, 1995). Powder diffraction data were collected from a conventional X-ray source.

Diffraction Line-Broadening Analysis

Microstructural imperfections (lattice distortions, stacking faults) and the small size of crystallites (i.e. domains over which diffraction is coherent) are usually extracted from the integral breadth or a Fourier analysis of individual diffraction line profiles. Lattice distortion (microstrain) represents a departure of atom positions from an ideal structure. Crystallite sizes covered in line-broadening analysis are in the approximate range 20–1000 Å. Stacking faults may occur in close-packed or layer structures, e.g. hexagonal Co and ZnO. The effect on line breadths is similar to that due to crystallite size, but there is usually a marked *hkl*-dependence. Fourier coefficients for a reflection of order l, $C(n,l)$, corrected from the instrumental contribution, are expressed as the product of real, order-independent, size coefficients $A^S(n)$

and complex, order-dependent, distortion coefficients $C^{D}(n,l)$ $[=A^{D}(n,l) + iB^{D}(n, l)]$. Considering only the cosine coefficients $A(n,l)$ $[=A^{S}(n)\cdot A^{D}(n,l)]$ and a series expansion of $A^{D}(n,l)$, $A^{S}(n)$ and the microstrain $\langle e^{2}(n)\rangle$ can be readily separated, if at least two orders of a reflection are available, e.g. from the equation

$$A(n,l) = A^{S}(n) - A^{S}(n)2\pi^{2}l^{2}n^{2}\langle e^{2}(n)\rangle$$

The inverse of the initial slope of the size coefficients $A^{S}(n)$ versus the Fourier harmonic number n (or $L=n/\Delta s$, where Δs is the range of the intrinsic profile in reciprocal units) is a measure of the Fourier apparent size, ε_F, defined as an area-weighted crystallite size. The second derivative of $A^{S}(n)$ is a measure of the crystallite size distribution in a direction perpendicular to the diffracting plane *hkl*, obtainable when strains are negligible. Fourier coefficients $C(n)$ are also related to the integral breadth, expressed in reciprocal units, β^{*} $[=\Delta s/\Sigma_{n}|C(n)|]$. For strain-free materials the reciprocal of this quantity is the integral-breadth apparent size, ε_{β}, defined as a volume-weighted thickness of a crystallite in the direction of the diffraction vector. For a spherical crystallite the direction of the diffraction vector is unimportant and there is a simple relation between the diameter D and ε_{β} $(=3D/4)$ or ε_F $(=2D/3)$. The ideal ratio $\varepsilon_{\beta}/\varepsilon_F$ is 1.125. Any departure from this ratio is due to the presence of a distribution of crystallite sizes. Similar expressions have been derived for other crystallite shapes, e.g. the cylinder, for which the two limiting cases are acicular and disk-like forms. Anisotropic models require precise determination of apparent sizes in various crystallographic directions. Representative examples of average spherical and cylindrical crystallite shapes are found in CeO_2 and ZnO loose powders.

These methods can be applied to more diffraction lines when profile-fitting techniques are employed, provided the observed data are precisely modelled. A more-detailed (three-dimensional) characterization of the microstructure can then be obtained. In the Fourier approach, line profiles must be reconstructed analytically, from the line-profile parameters extracted from pattern-decomposition techniques, prior to the physical interpretation. With the integral-breadth method, the use of Voigt functions in the modelling of observed h and instrumental g profiles represents a definitive advantage, since the integral breadth β_f of the intrinsic f profile can be precisely determined. Whatever the diffraction-line-broadening analysis employed, an essential preliminary step in the analysis is to examine a (Williamson–Hall) plot giving the variation of β_f (expressed in reciprocal units) as a function of d^{*}. Although this plot is not used for quantitative characterization, it gives an overview of the nature of the broadening due to sample imperfections and orients the subsequent analysis. Figure 6 shows the

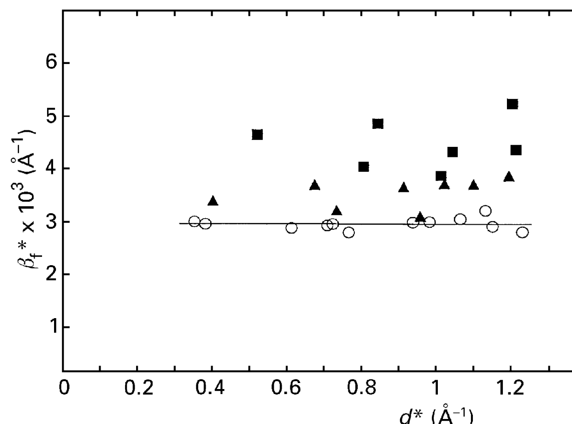

Figure 6 Example of a Williamson–Hall plot for a sample of nanocrystalline ZnO powder exhibiting size and stacking-fault diffraction line broadening according to the *hkl* values. (○) reflections unaffected by mistakes (*hk*0 and *hkl* with *l* even, $h-k=3n$), (▲) first reflection set affected by stacking faults (*hkl* with *l* odd, $h-k=3n\pm1$), (■) second reflection set affected by stacking faults (*hkl* with *l* even, $h-k=3n\pm1$).

hkl-dependence of the integral breadths for a sample of nanocrystalline ZnO. These plots can be varied according to the effects at the origin of line broadening and to their anisotropic nature. Since perfect modelling of line profiles are required in the Rietveld method, the technique can also, in principle, be used to extract microstructural properties. However, unless line broadening is isotropic, to obtain meaningful information the procedure must be able to handle the various possible sources of broadening present in the pattern, such as crystallite size, strain, stacking faults, dislocation density, and the residual errors related to the structure and preferred orientation models must be minimized.

Dynamic and Non-ambient Diffraction

Time and temperature dependent X-ray diffraction includes the measurement of a series of diffraction patterns as a function of time, temperature or other physical constraint. The time required for collecting data decreases considerably with the availability of fast detectors, such as PSDs, and the brightness of the X-ray source. In principle, line-profile parameters can be extracted for each pattern and interpreted in structural (peak position and integrated intensity) and microstructural (breadths and line shapes) terms. Consequently, the structural and microstructural changes taking place as a function of the external constraint (temperature, atmosphere, pressure, electric field, etc.) are displayed from the successive patterns. The method affords the possibility of establishing the pathways during chemical solid-state reactions, such as phase transition and

thermal decomposition, and to determine the kinetics of processes, e.g. the crystallization of nanocrystalline solids or phase transformations. Patterns can be collected on a time scale of a few minutes with conventional X-rays but the high brightness of synchrotron radiation makes it possible to measure diffraction data in very short time periods. A representative application is the investigation of fast and self-propagating solid combustion reactions on a subsecond time-scale. *In situ* powder diffraction can also be combined with other complementary techniques applied simultaneously, such as EXAFS (extended X-ray absorption fine structure). The two structural probes may provide long-range order information (powder diffraction) and short-range order details (EXAFS). For instance, *in situ* combined X-ray diffraction and EXAFS have been used for the study of the formation of heterogeneous catalysts.

See also: Inorganic Compounds and Minerals Studied Using X-Ray Diffraction, Materials Science Applications of X-Ray Diffraction, Neutron Diffraction, Theory, Small Molecule Applications of X-Ray Diffraction, X-Ray Absorption Spectrometers.

Further Reading

Bish DL and Pose JE (eds.) (1989) *Modern powder diffraction. Reviews in Mineralogy*, 20: 1–369.
Harris KDM and Tremayne M (1996) Crystal structure determination from powder diffraction data. *Chemistry of Materials* 8: 2554–2570.
Jenkins R and Snyder RL (1996) *Introduction to X-ray Powder Diffractometry*. New York: Wiley.
Langford JI and Louër D (1996) Powder diffraction. *Reports on Progress in Physics* 59: 131–234.
McCusker LB, Von Dreele RB, Cox DE, Louër D, and Scardi P (1999) Rietveld refinement guidelines. *Journal of Applied Crystallography* 32: 36–50.
Parrish W (1995) Powder and related techniques: X-ray techniques. In: Wilson AJC (ed.) *International Tables for Crystallography*, vol. C, pp. 42–79. Dordrecht: Kluwer Academic Publishers.
Smith DK (1997) Evaluation of the detectability and quantification of respirable crystalline silica by X-ray powder diffraction methods. *Powder Diffraction* 12: 200–227.
Young RA (ed.) (1995) *The Rietveld Method*. Oxford: IUCr-Oxford University Press.